Vol. 38, No. 1
March 2020

JOURNAL OF
RADIATION
EFFECTS
Research and Engineering

Irradiation Effects on the Performance of III-V-Based nBn Infrared Detectors

C.P. Morath, E.H. Steenbergen, G.D. Jenkins, and D. Maestas

This paper was presented at the 36th Annual HEART Conference
San Diego, CA, April 8–12, 2019.

Prepared by Amentum for the HEART Society under contract to NSWC Crane

This work was sponsored by the Air Force Research Laboratory Space Vehicles Directorate.

JOURNAL OF RADIATION EFFECTS,
Research and Engineering
Vol. 38, No. 1, March 2020

IRRADIATION EFFECTS ON THE PERFORMANCE OF III-V-BASED nBn INFRARED DETECTORS

C.P. Morath, E.H. Steenbergen, G.D. Jenkins, and D. Maestas
Air Force Research Laboratory Space Vehicles Directorate
Kirtland AFB, NM

Abstract

Progress towards understanding the effects of irradiation on the performance of III-V-based nBn and other barrier-architecture infrared (IR) detectors over the last decade is reviewed and the mechanisms underlying the observed performance degradation are discussed. Detector performance degradation was quantified by observing changes in three performance parameters: 1. lateral optical collection length, 2. quantum efficiency, and 3. dark-current density. Examining the theoretical equation for quantum efficiency damage factor suggested that increasing the minority-carrier mobility would enhance the radiation tolerance. Measurements of the radiation tolerance of a new nBn-related detector, the p-insert, where both holes and higher mobility electrons are photo-generated minority carriers, align with that prediction.

Introduction

The nBn infrared (IR) detector has made sustained progress since its introduction over a decade ago and spawned a whole new class of minority-carrier photodetectors based around the use of "unipolar barrier layers" [1], [2]. A unipolar barrier layer is made from a novel semiconductor heterostructure type I alignment where one energy band, either the conduction or valence band, is continuous across the heterointerface. Thus, the barrier layer either has a zero conduction or valence band offset and thereby blocks one carrier type (electron or hole) while allowing an unimpeded flow of the other. In the *nBn* IR detector, for example, an electron unipolar barrier *B* blocks the majority carrier electron current between the two *n* regions sandwiching it; conversely, in a *pBp* detector, a hole unipolar barrier *B* blocks the majority carrier hole current between two *p* regions sandwiching it. The doped layers in each serve as a contact layer and absorbing layer, respectively.

As the electron barrier layer in the nBn detector is formed using relatively wider-bandgap semiconductor material, it also ideally eliminates the formation of a depletion region in the active n region next to it, when the nBn is biased. Simultaneously, the same electron barrier also happens to block the n-type surface current that typically arises on mesa surfaces of III-V materials. Thus, the electron barrier layer limits the possible dark-current mechanisms in nBn detectors to diffusion current associated with recombination processes in the narrow gap layer. This reduction in dark-current mechanisms leads to nBn detectors with similar performance to a conventional photodiode from the same material operating at lower operating temperatures or better performance than the photodiode at the same operating temperature. This performance improvement has already led to the adoption of nBn detectors in place of conventional IR photodiode technology for terrestrial defense applications such as the F-35 program [3].

As nBn technology has progressed substantially with a growing domestic industrial base, it is now also being considered for demanding space defense applications such as missile warning and space surveillance. The conventional, high-performance IR detector material for these space applications is mercury cadmium telluride (HgCdTe); however, HgCdTe technology remains limited by the availability, size, and cost of high-quality, large-format cadmium zinc telluride (CdZnTe) substrate material. The narrow-gap absorbing material in nBn detectors is from the 6.1 Å family of III-V compounds (indium arsenide [InAs], aluminium antimonide [AlSb], and gallium antimonide [GaSb]); thus, nBns can be grown on relatively more readily available, and hence cheaper, GaSb and gallium arsenide (GaAs) substrate materials. This among several other reasons makes them a

This work was sponsored by the Air Force Research Laboratory Space Vehicles Directorate.

potential alternative to HgCdTe, especially for use in a possible future proliferated space-sensor layer where very large numbers of less costly sensors may be present [4]. The space environment, however, places the most stringent performance requirements on an IR-detector array due to the larger imaging distances and consequent lower signal levels. Space also adds the unique requirement for detector radiation tolerance, which can limit possible orbits and total mission lifetime.

Hence, several recent investigations were undertaken to understand the effects of gamma and proton irradiation on nBn detectors [5], [6]. A further study analyzing empirical trends of the proton irradiation damage factors of nBn detectors indicated they have significant dependence on the detector properties and operating conditions and suggested a new methodology for comparing the rad-tolerance of these detectors [7]. The quantum efficiency of the nBn detector was then shown to have a near-linear inverse dependence on proton fluence, prompting the definition of a new, more accurate quantum efficiency damage factor [8]. Another study attempted to detail the effects of proton irradiation on the dark current in nBn detectors [9]. Significant issues with the proton irradiation results in this study were re-analyzed in a later report, which showed that proton irradiation may lead to an increase in n-type carrier population as well as limiting how fast the dark current increases with proton fluence [10]. Finally, several related studies on the dependence of minority-carrier lifetime in nBn IR materials on proton irradiation were also recently undertaken [11]–[14].

Here, the recent progress toward understanding the effects of gamma and proton irradiation on the performance of III-V-based nBn and other barrier architecture IR detectors is reviewed. Simple device physics expressions were used to account for the degradation of the measured detector performance due to irradiation. The detector performance was quantified in terms of measured lateral optical collection length, quantum efficiency, and dark current. Furthermore, some new results from a proton irradiation experiment on an nBn-related detector called the p-insert were also presented. These results demonstrated the possibility for mitigating the typical proton irradiation-induced degradation of detector quantum efficiency seen in nBns to some degree by using higher mobility electrons, in addition to lower mobility holes, as photo-generated minority carriers that generate the photocurrent. Thus, this result supported expectations about the nBn quantum efficiency damage factor being a direct function of its minority-carrier mobility, which is subject to localization effects in the vertical growth direction making it extremely small at low temperatures [15], [16].

Background

The principles of operation for the nBn detector were fully described in [1], [17], and [18] and are briefly reviewed again here. The first barrier detector concept was proposed by A.M. White in 1983 as a high-impedance photoconductor and postulated a heterostructure consisting of a relatively thin barrier layer with near-zero-valence-band offset sandwiched between a narrow-gap absorber region and contact region [19]. It was well over a decade later that the first nBn detectors were independently realized using III-V materials, the first publicly reported in [1] using InAs as the absorber material.

A schematic of the energy band diagram of an nBn IR detector under an applied external voltage V_{bias} is shown in Fig. 1 [20]. Here, the nBn is illuminated through the substrate, which is often completely removed to prevent any optical loss there. If an incoming photon (red squiggle arrow) is absorbed in the absorber layer, the resulting photo-excited electron and hole diffuse in opposite directions to generate the photocurrent J_{SIG}, which represents the

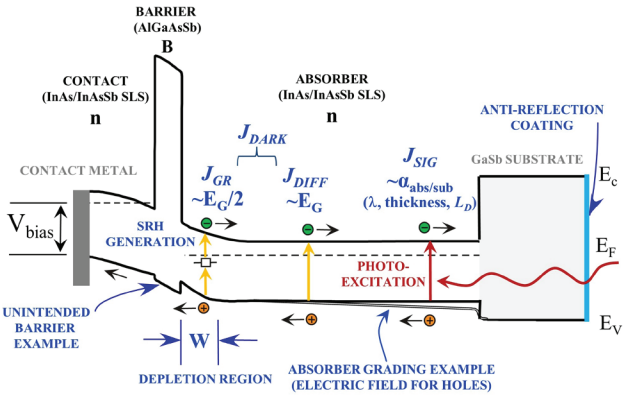

Figure 1. Schematic of the energy band diagram of an nBn IR detector under an external applied V_{bias} showing the relative locations of each layer, photo-excitation process, majority- and minority-carrier motion, typical dark-current and photocurrent mechanisms, quasi-Fermi levels, and biasing effect. An ideal nBn detector has a depletion width $W = 0$ and zero-valence-band offset or unintended barrier for hole transport [20].

detector signal. This absorption process is characterized by the absorption coefficient α and thickness L_A of the absorbing region. The α is a function of the bandgap energy E_G of the narrow-gap absorber layer and the wavelength λ of the incoming light.

The excess minority holes generated by absorption must diffuse across the absorber layer and past the high-field barrier layer, prior to recombining, to be collected as photocurrent. Recombination of the photo-generated carriers is typically limited by the Shockley-Read-Hall (SRH) recombination process (not shown), which is characterized by the minority-carrier lifetime τ. The rate of the hole diffusion is characterized by the diffusivity D, given by the Einstein Relationship $D = (k_B T \mu_h / q)$, where k_B is Boltzmann's constant, T is the temperature, q is the electron charge, and μ_h is the minority-carrier hole mobility. The average distance an excess hole diffuses before recombining is given by its diffusion length $L_D = \sqrt{D\tau}$ (equivalently, L_D is also the rate parameter characterizing the decay of the equilibrium thermally generated, excess minority-carrier density $\delta p = p_n - p_{n0}$ with distance from the barrier-absorber heterostructure interface). Given the possibility for their recombination, the collection of diffusing holes is inherently probabilistic. This probability is reflected in the ratio L_D/L_A, which factors strongly into the proton irradiation tolerance.

The nBn detector noise is related to its dark current, which includes any other currents present aside from the photocurrent. Typical III-V photodiode detectors have three primary dark-current sources: 1. diffusion current of thermally generated carriers in the quasi-neutral absorber; 2. generation-recombination current of carriers thermally generated via SRH-centers in the depletion region; and 3. surface currents, both shunt and recombination, which arise due to side-wall passivation issues. The defining role of the electron barrier layer in the nBn detector is to eliminate sources 2 and 3 above. As the surfaces of III-V detector pixels are n-type due to Fermi-level pinning, all the surface currents are blocked by the electron barrier layer eliminating source (3 above). Source 2 is eliminated in the nBn detector because the applied bias voltage ideally falls only across the wider bandgap barrier layer, which leaves the narrow-band, n-type contact and absorber layers in the flat-band condition. The thermal generation in this barrier region is very low due to its much larger energy bandgap. In reality, however, a non-zero depletion width $W > 0$ may form near the barrier-absorber interface, as illustrated by the schematic in Fig. 1. This leads to some depletion or generation-recombinaton dark-current J_{Depl} associated with SRH-generation processes in the depletion region, which has a thermal-dependence $\exp(-E_G / 2k_B T)$, where E_G is the energy bandgap of the narrow-gap absorber layer.

Dark-current source remains present in nBn detectors, even in the ideal case, as the electron barrier layer does not block it. This diffusion dark-current J_{Diff} of thermally generated carriers in the quasi-neutral region is by definition a function of L_D and thus dependent on hole mobility and recombination lifetime. The latter, in turn, is typically limited by the SRH recombination process for these materials. The diffusion dark current in the nBn has a thermal-dependence $\exp(E_G / k_B T)$. Despite the 1/2-factor difference in their exponents, total dark current in an nBn detector is usually dominated by J_{Diff}, rather than J_{Depl}, in the temperature range of interest ($T > 80$ K) as $W \simeq 0$. Finally, the electron barrier layer also blocks the re-injected electron photocurrent current and the thermally generated electron diffusion current from the n-type contact layer (not shown). Thus, the nBn detector is essentially a minority-carrier photoconductor with unity gain similar to a photodiode, with the barrier replacing the junction (space charge region) and the p-contact replaced by an n-contact. For these reasons, the nBn may be considered a hybrid between a photoconductor and photodiode.

The schematic in Fig. 1 also illustrates the concept of an unintended valence-band offset and the so-called valence-band grading in the absorbing layer. The presence of any discontinuity of the valence-band energy from the barrier layer, either a positive (shown) or negative offset, limits the diffusing holes from generating J_{Sign} as both act as unintended barriers. The offset necessitates higher turn-on voltages to generate the photocurrent, which are undesirable as they also lead to $W > 0$. Valence-band grading in the absorber layer implies a continuously varying increase in E_G as shown. This leads to a small electric field E being applied only to the holes, enhancing their ability to be collected as photocurrent before recombining. Thus, grading also has implications for the rad-tolerance of the nBn detector. In the presence of a

graded valence band, an effective diffusion length $L_{Eff} = L_D(EL_{Dq}/k_BT)$ replaces L_D [21] as the relevant parameter.

Theory and Results

In this section, simple analytical one-dimensional (1-D) theory and various measurement results are used to elucidate the effects of proton-irradiation on the performance of nBn detectors [8]. Proton irradiation of semiconductor materials and devices leads to both displacement and ionization damage. In nBn detectors, however, only displacement damage typically has measurable effects as discussed below. Displacement damage occurs when the incoming radiation particle transfers sufficient energy to an atom during an elastic or inelastic nuclear collision to knock it from its lattice site creating both a vacancy (V) and interstitial (I) defect [22]. These defects act as additional minority-carrier-recombination sites, which reduce the minority-carrier lifetime τ in semiconductor materials according to $\tau^{-1} = (\sigma \upsilon_{th} N_T)$, where σ is the minority-carrier-capture cross section, υ_{th} is the thermal velocity, and N_T is trap concentration that is proportional to proton fluence Φ_P [14].

Ionization damage is the creation of excess electron-hole pairs as the incoming radiation particle loses its energy through ionizing interactions. In electronic semiconductor devices, these excess carriers may become trapped in passivating dielectric layers or on the surfaces of mesa devices. For detector pixels, ionization damage thus typically manifests as higher surface current, which is a source of dark current. However, for nBn detector pixels, the effects of ionization damage on the performance are typically small enough to be ignored due to the presence of the electron barrier layer, which is highly effective at blocking the n-type surface currents generated by ionization damage.

An example of ionization damage in a midwave-infrared (MWIR) nBn detector, from the very first reported irradiation experiment on any nBn detector, is shown in Figs. 2 and 3 from [5]. The first figure shows the increase in pixel dark-current density J_D as a function of gamma irradiation dose up to 200 krad(Si). The data show only a ~2.6% increase in J_D over this entire range, which is difficult to discern clearly given the level of uncertainty present. The sources of uncertainty in these measurements, which based on the apparent maximum point-to-point variation at TID < 20 krad(Si) is ~1%, are likely the mechanism itself governing the generation of additional surface charge in the detector due to the gamma irradiation and any possible thermal annealing over time that might occur. Both of these are difficult to predict and influenced by the quality of the original mesa surfaces, which varies depending on the quality of the semiconductor processing.

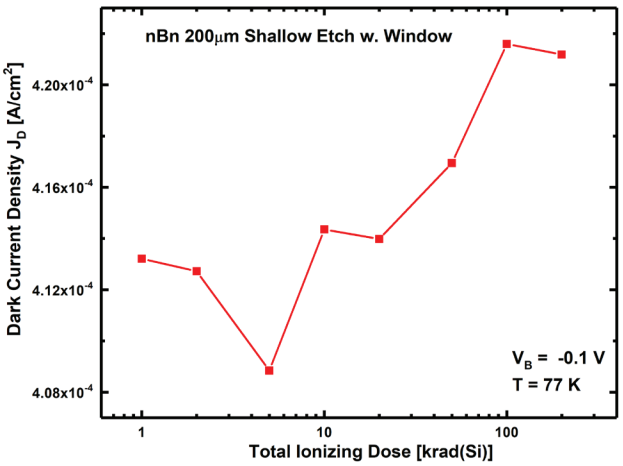

Figure 2. Example of ionization damage on dark current in an nBn detector showing only a small increase for gamma irradiation up to 200 krad(Si) [5].

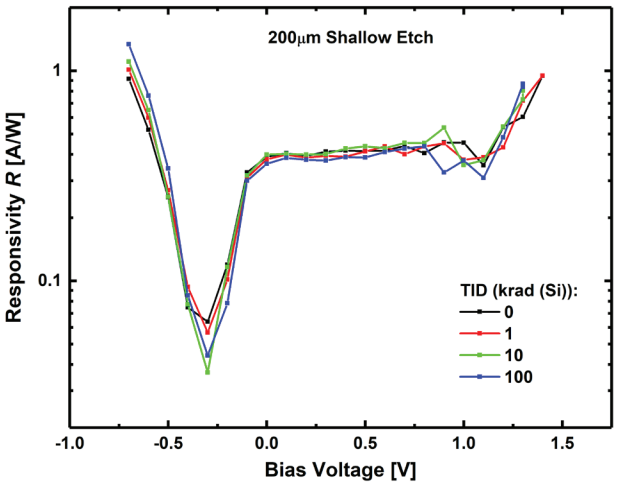

Figure 3. Example of ionization damage on responsivity, and hence photocurrent, in the same nBn detector as Fig. 2 showing no measurable change under gamma irradiation up to 100 krad(Si) [5].

Fig. 3 indicates no measurable change was observed, as expected, in detector responsivity, and hence photocurrent, for the same nBn detector as in Fig. 2 over the dose range up to 100 krad(Si). The uncertainty present in this data, which appears < 1%, is likely due to

fluctuations of the temperature of the blackbody source that was used to illuminate the detector under test to generate the photocurrent. These results reflect how ionization damage does not manifest in the optical response of a detector. Similar results as these were obtained in more recent gamma irradiation experiments on nBn IR focal plane arrays [23]. Thus, nBn detectors are expected to be very tolerant to gamma irradiation and hence ionization damage, which is traceable to their electron barrier layer that effectively blocks the n-type surface currents.

As described in [7], optical characterization of a set of detector pixels of variable area using flood illumination through a limiting round aperture held at a known distance from the sample allows for both the 1-D, bulk-limited quantum efficiency η and the lateral optical collection length L_{OC} to both be ascertained from a plot of the square root of the measured photocurrent $\sqrt{I_P}$ versus the mesa length L. Given ideal, uniformly responding pixels, this plot is expected to show a relatively linear relationship where $\eta = m^2/qE_q$, $L_{OC} = b/2m$, m and b are the slope and y-intercept of the aforementioned plot, respectively; E_q is the calculated irradiance; and q is electronic charge. L_{OC} effectively defines the area outside the established mesa-defined pixel area from which photogenerated carriers may be collected via lateral diffusion and generate additional photocurrent. Thereby, the true pixel optical area is effectively $(L+2L_{OC})^2$. This approach to detector optical characterization has the benefit of isolating the individual degradations of η and L_{OC} due to proton-irradiation, which is necessary since both cause degradation of the overall measured photocurrent [24]. The same lateral diffusion process from off-mesa area that accounts for L_{OC} likewise impacts the dark current and necessitates performing a perimeter-to-area analysis of dark-current measurements from variously sized pixels to ascertain the true 1-D, bulk-limited dark current.

The degradation of L_{OC} for nBn detectors undergoing displacement damage was detailed in [7]. Summarizing, L_{OC} was shown to be proportional to L_D in [25] and thus $L_{OC}^2 \propto \tau$. For nBn materials, the minority-carrier hole recombination lifetime is again given by $\tau^{-1} = \sigma v N_T$, where the defect density is $N_T \propto \Phi_P$, the proton fluence, for the range and energies of interest. Under proton irradiation, L_{OC}^{-2} is thus expected to increase linearly with increasing Φ_P, similar to $1/\tau$[14]. An optical collection length damage factor $K_{L_{OC}^{-2}}$ is defined as the slope of this linear increase. Fig. 4 shows a typical example of L_{OC}^{-2} increasing with Φ_P for an MWIR nBn detector undergoing step-wise 63-MeV proton irradiation up to $\Phi_P \sim 5.3 \times 10^{11}$ p/cm^2. This plot indicated N_T increased linearly with Φ_P, as expected, over this entire fluence range and that L_{OC} recovered to near its $\Phi_P \sim 2.65 \times 10^{11}$ p/cm^2 level following a multi-day, 300-K thermal anneal.

In an IR focal plane array, where the pixels are all identically sized, L_{OC} may contribute to the pixel photocurrent depending on the pixel design. Thus, obtaining the proton-radiation tolerance of L_{OC} separately using variably sized pixels, as described in the process above, is often worth doing in and of itself. Practically speaking, however, measuring the expected linear change in L_{OC}^{-2} with increasing Φ_P, as shown in Fig. 4, is a means to ascertain whether the rate of defect formation under proton irradiation has varied during the course of the experiment. Additionally, L_{OC} is dependent on both fit parameters m and b in the measurement process described above, so L_{OC} is very sensitive to any changes in the optical measurement itself such as fluctuations in the blackbody source or a shift in the dewar position during testing. Together, this makes tracking the expected change of L_{OC}^{-2} invaluable during an nBn detector radiation tolerance experiment.

The degradation of an nBn detector's quantum efficiency η undergoing displacement damage due to proton irradiation can be substantial as described in [8].

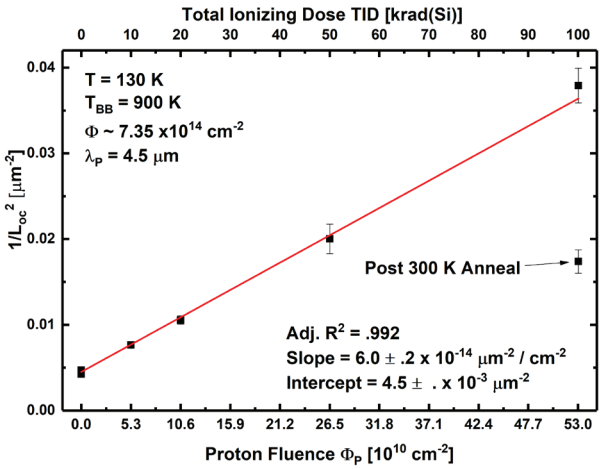

Figure 4. Example of linear relationship between L_{OC}^{-2} and increasing Φ_P for a typical MWIR nBn detector undergoing step-wise 63-MeV proton irradiation up to $\Phi_P \sim 5.3 \times 10^{11}$ p/cm^2. Post 300-K anneal point reflects a multi-day thermal anneal was performed.

From the section above, the 1-D, bulk-limited detector quantum efficiency η is most accurately determined from a set of photocurrent measurements on variably sized detector pixels using a process that separates the vertical collection of photo-generated carriers from any lateral collection. This approach has the additional advantage that the experimentally determined trends for η with increasing Φ_P are comparable with trends determined from simple, analytic, 1-D theory. Hereby, an approach to theoretically understand the degradation mechanism for η is provided.

The following expression from Van de Wiele [26] is for the quantum efficiency of a 1-D, quasi-neutral absorbing region in semiconductor photodiode and is applicable to η of an defect formation nBn detector:

$$\eta_{qn} = \left(\frac{\alpha^2 L_D^2}{1-\alpha^2 L_D^2}\right)\left\{e^{-\alpha L_A} - \frac{1}{\cosh(L_A/L_D)} + \frac{e^{-\alpha L_A}\tanh(L_A/L_D)}{\alpha L_D}\right\}. \quad (1)$$

From the first term, in parentheses, of the inverse of (1), which is given by

$$\frac{1}{\eta_{qn}} = \left(\frac{1}{\alpha^2 L_D^2} - 1\right)\left\{e^{-\alpha L_A} - \frac{1}{\cosh(L_A/L_D)} + \frac{e^{-\alpha L_A}\tanh(L_A/L_D)}{\alpha L_D}\right\}^{-1}, \quad (2)$$

it is apparent that $1/\eta_{qn} \propto 1/\tau$ and would degrade likewise if the second term in parenthesis in (2) was ignored. As shown by modeling in [8], it turns out that the effect of the second term in (2) on the linearity of the first term is mostly negligible; its role is mainly to ensure $\eta_{qn}^{-1} > 0$. This expectation is reflected in the data in Fig. 5, where $1/\eta_{qn}$ versus Φ_P is plotted for the same nBn detector as in Fig. 4. Thus, a quantum efficiency damage factor $K_{\eta^{-1}}$ may be defined by the slope of this linear dependence.

Like Fig. 4, the post-300-K anneal data point in Fig. 5 reflects recovery of η following a multi-day 300-K anneal back to a roughly similar level near its ~ 2.65×10^{11} p/cm^2 level. Recovery of τ to this level in similarly proton-irradiated nBn materials following a multi-day 300-K anneal was also routinely observed, as shown by the example in Fig. 6 from [14]. Here, τ itself was directly measured as a function of proton fluence using time-resolved photoluminescence (PL) of the bare material. The uncertainty in these lifetime measurements, which was low given the clearly linear behavior, is mostly due to the ability to fit the PL-decay as it becomes significantly weaker at higher doses.

The matching trends between Figs. 4, 5, and 6 clearly indicate that degradation of τ due to an increase in N_T from increasing Φ_P is the source of all the detector performance degradation under proton irradiation. The slope of τ^{-1} in Fig. 6 is taken as the lifetime damage factor $K_{\tau^{-1}}$, which is theoretically given by the following:

$$K_{\tau^{-1}} = \sigma\nu\left(\frac{dN_T}{d\Phi_P}\right). \quad (3)$$

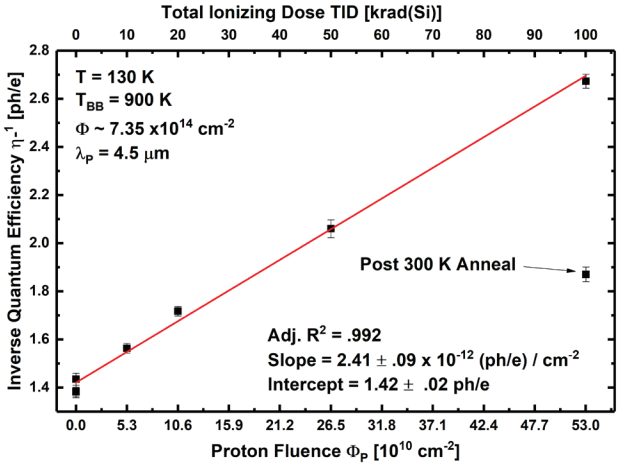

Figure 5. Example of η degradation with proton irradiation for the same MWIR nBn detector as in Fig. 4. Data are re-plotted as η^{-1} versus increasing Φ_P and linear fitting suggests a damage factor $K_{\eta^{-1}}$ equal to the slope.

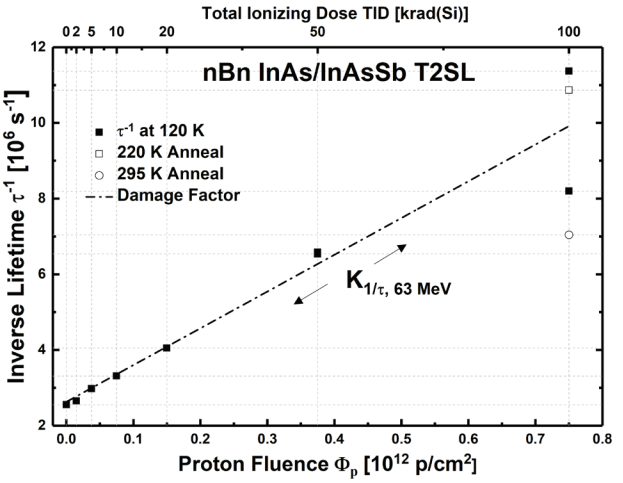

Figure 6. Example of τ^{-1} degradation with proton irradiation for typical MWIR nBn detector material. The 295-K anneal data point reflects recovery to roughly the same level as in Figs. 4 and 5 following a multi-day thermal anneal [14].

Further algebraic manipulation of the first term in (2) reveals that $K_{\tau^{-1}}$ is related to $K_{\eta^{-1}}$ according to

$$K_{\eta^{-1}} \propto \frac{K_{\tau^{-1}}}{\alpha^2 D} = \frac{qK_{\tau^{-1}}}{\alpha^2 \mu k_B T}. \quad (4)$$

This equation indicates that higher minority-carrier mobility μ leads to both higher initial η and lower $K_{\eta^{-1}}$ during proton irradiation and vice-versa; higher absorption coefficient α and temperature T would clearly act likewise. It is important to mention here that this mobility relates to the direction of the carrier motion and in an nBn detector pixel that carrier motion is vertical, along the material growth axis.

For III-V-based superlattice IR materials, which are used for nBn IR detectors, the vertical mobility will clearly be different from the lateral mobility as the band structure along the growth axis is very different due to the presence of the heterointerfaces. Vertical hole mobility μ in III-V superlattice nBn materials was measured and revealed to be unexpectedly low due to localization effects [27]. This initial result was recently confirmed using vertical magnetotransport measurements on nBn IR materials [15], [16]. This work also showed vertical electron mobility in these materials was nearly 3 orders higher at 130 K, which based on (2) suggests using a p-type absorbing layer would take advantage of the electron as the minority carrier and reduce $K_{\eta^{-1}}$.

Evidence for the improvement in η-degradation by using higher mobility electrons as minority carriers was apparent in the results of a recent investigation of the rad-tolerance of a so-called p-insert detector. This is effectively an MWIR nBpn detector, where a p-layer has been *inserted* into the n-type absorbing layer. Thus, this detector is a close cousin to the nBn detector although it has markedly different proton-radiation tolerance behaviors as shown in Fig. 7.

The main difference between the nBpn and nBn detectors is that the purpose of the barrier layer in the former is reduced to simply blocking the n-type surface current. For the p-insert detector, it is expected that quasi-neutral regions on either side of the pn junction contribute to the photocurrent and thus, under proton irradiation, the η's of each region should both degrade. Given its higher-mobility, n-type minority carriers, the p-region's η-degradation should be far smaller than the n-region's. The plot of η^{-1} in Fig. 7 is consistent with this expectation. It shows a significant initial decay, which is likely due to the quicker degradation of the photocurrent generated in the n-type region. This is followed by a saturation region, which is likely due to the non-degrading photocurrent generated in the p-type region. The uncertainty bars on the measurements in Fig. 7, which are clearly much larger than those in Fig. 5, likely reflect the smaller number of variably sized detectors that were used to determine η and the poorer uniformity of all those detectors on the same test chip. As described above, η is experimentally determined by fitting $\sqrt{I_P}$ vs. L; thus, the fewer data points and larger spread of data would statistically contribute to these larger uncertainties. The large uncertainty is thus a manifestation of the poorer quality of the detector test chip; this poorer quality is also reflected by the larger values for η^{-1} in Fig. 7 compared to Fig. 5. The consistency of the measurement scheme, however, is demonstrated by the apparent trends of η^{-1} in Fig. 7. These data were collected over multiple days, and for each dose step, the test dewar was moved in front of the proton beam and then returned to the test station for measurement following the dose. To ensure consistent illumination of the detectors, both the test dewar and blackbody source used individual kinematic mounts that were secured to the optical table, and the temperature of the blackbody source was monitored.

Under proton irradiation, the dark current of the standard nBn detector increases, but ideally remains

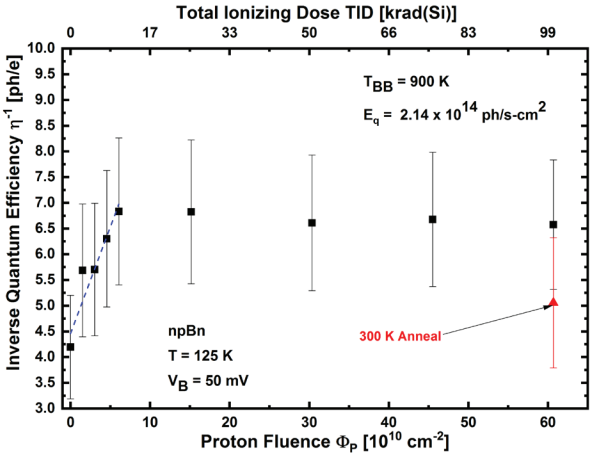

Figure 7. Example of $1/\eta$ degradation with proton irradiation for an MWIR nBpn detector, the so-called p-insert. Saturation-behavior for $\Phi_P > 5\times10^{10}$ cm^{-2} suggests the higher mobility n-type carriers in the p-insert region are limiting further degradation of η.

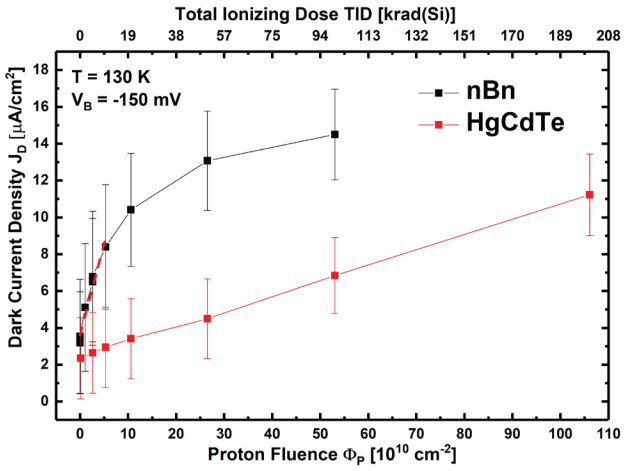

Figure 8. Example of J_D degradation with proton irradiation for an MWIR nBn detector and HgCdTe photodiode [14].

diffusion-limited as the width of the depletion region remains negligible and the barrier continues to block surface currents [9]. In contrast, in typical MWIR photodiodes a combination of increased depletion-current and/or surface-currents arise, albeit still typically more slowly than the measured increase in diffusion-limited dark current of an nBn detector for similar cutoff wavelengths. This difference is clearly illustrated by the results in Fig. 8 from [14] where markedly different behaviors are observed for each. The HgCdTe photodiode's J_D appears to increase linearly with increasing Φ_P, while the nBn detector's J_D shows a saturation-like behavior.

The increase in an nBn's diffusion dark current is still due to degradation of its SRH-limited τ, exactly similar to η and L_{OC}. This characteristic of the nBn detector to remain diffusion-limited as $\tau \rightarrow 0$ led to the unique expectation for J_D to undergo a transition in its dependence on Φ_P as irradiation increased and L_D decreased from $L_D \gg L_A \rightarrow L_D \ll L_A$, where L_A is the absorber width [9].

To examine this, the well-known expression from Van de Wiele for the diffusion current of a one-sided photodiode, which is analogous to the nBn detector, is considered in the following [26]. The expression for this diffusion-current, assuming a zero-surface recombination velocity $S = 0$, is given by the following [9]

$$J_{Diff} = \frac{qn_i^2}{N_D}\frac{D}{L_D}\tanh\left(\frac{L_A}{L_D}\right). \quad (5)$$

This reduces to $J_{Diff} \approx q(n_i^2/N_D)(L_A/\tau)$ for $L_D \gg L_A$ and $J_{Diff} \approx q(n_i^2/N_D)\sqrt{D/\tau}$ for $L_D \ll L_A$. The former approximations for J_D has a linear-dependence on Φ_P due to the τ^{-1}-dependence, while the latter approximation has a square root dependence on Φ_P due to the $\tau^{-1/2}$-dependence. Thus, as L_D transitions from $L_D \gg L_A \rightarrow L_D \ll L_A$, a strong change in J_D's dependence on Φ_P is expected.

Dark-current data from a 500-μm MWIR nBn detector on the same sample used to generate Fig. 4 and 5b in [9] are shown in Fig. 9(a). In 9(b), J_D calculated from that data at various bias voltages is plotted versus increasing 63-MeV proton fluence Φ_P. At every V_B, the J_D appears to increase

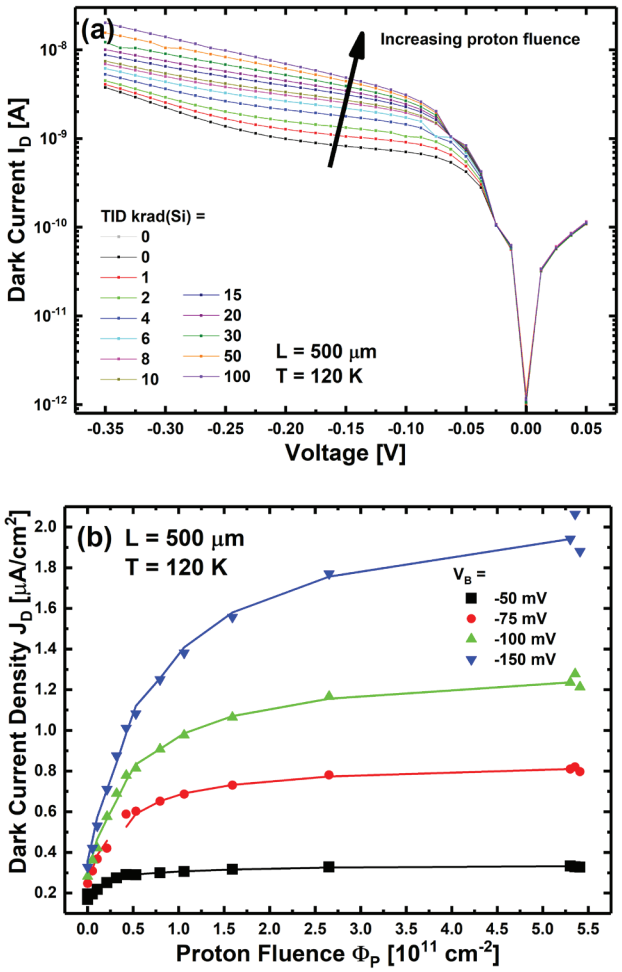

Figure 9. (a) Example of a 500-μm MWIR nBn detector's dark current vs. bias voltage at T = 120 K as function of irradiation by 63-MeV protons at fluences ranging from 0 → 5.3 x 10^{11} cm^{-2}; (b) J_D calculated from data in (a) vs. Φ_P at various V_B. $J_D(\Phi_P)$ transitions from $(L_D \gg L_A) \rightarrow (L_D \ll L_A)$-limits as it initially increases rapidly and then begins saturating for Φ_P > .5 x 10^{11} cm^{-2} [10].

rapidly at low Φ_P and become near-saturated at higher Φ_P, suggesting a transition from ($L_D \gg L_A$) to ($L_D \ll L_A$) regimes has likely occurred.

However, the near-saturation behavior of J_D at higher fluences in Fig. 9 is increasing much too slowly to follow the expectation from the approximation above, $J_D \propto \Phi_P^{1/2}$. This result was determined to be due to an increase in n-type doping density N_D that accompanied the degradation of τ and, which according to (5), would lead to slower increase in J_{Diff} [10]. The increase in N_D with increasing proton fluence was independently measured by capacitance-voltage measurements, and the carrier addition rate was found through modeling to be sufficient to lead to a noticeable decrease in the rate of the increase in J_{Diff}.

Conclusion

A review to date of various aspects of the degradation of performance of nBn IR detectors, including their L_{OC}, η, and J_D due to irradiation, was provided. New results on the so-called p-insert detector, a close cousin to the nBn, suggested that using the electron as the minority carrier improves the rad-tolerance of the quantum efficiency in III-V-based IR detectors, which is a significant current concern for the space-based detector community.

Acknowledgment

The authors acknowledge discussions with Dr. John E. Hubbs and Dr. Lilian Casias regarding measurements and development of these ideas herein as well as the support of the Air Force Research Lab Space Vehicle's Directorate leadership.

References

[1] S. Maimon and G. Wicks, "nBn detector, an infrared detector with reduced dark current and higher operating temperature," *Appl. Physics Lett.*, vol. 89, no. 151109, 2006.

[2] P. Klipstein, "'XBn' barrier photodetectors for high sensitivity and high operating temperature infrared sensors," *Proc. SPIE*, vol. 6940, no. 69402U, 2008.

[3] M. Tidrow *et al.*, "III-V SLS FPA development after VISTA," presented at *QSIP 2018*, June 2018.

[4] J. Judson, "MDA director provides rough sketch of possible space-based missile defense sensor layer," *Defense News*, 2018. [Online]. Available: https://www.defensenews.com/

[5] V.M. Cowan *et al.*, "Gamma-ray irradiation effects on InAs/GaSb-based nBn IR detector," *Proc. SPIE*, vol. 7945, no. 79451S, 2011.

[6] V. Cowan *et al.*, "Radiation tolerance characterization of dual band InAs/GaSb type-II strain-layer superlattice pBp detectors using 63 MeV protons," *Appl. Physics Lett.*, vol. 101, no. 251108, 2012.

[7] C.P. Morath, V.M. Cowan, L.A. Treider, G.D. Jenkins, and J.E. Hubbs, "Proton irradiation effects on the performance of III-V-based, unipolar barrier infrared detectors," *IEEE Trans. Nucl. Sci.*, vol. 62, no. 2, pp. 512–519, 2015.

[8] C.P. Morath, E.A. Garduno, G.D. Jenkins, and V.M. Cowan, "More accurate quantum efficiency damage factor for proton-irradiated, III-V-based unipolar barrier infrared detectors," *IEEE Trans. Nucl. Sci.*, vol. 64, no. 1, pp. 74–80, 2017.

[9] G.R. Savich *et al.*, "Diffusion current characteristics of defect-limited nBn mid-wave infrared detectors," *Appl. Physics Lett.*, vol. 106, p. 173505, 2015.

[10] C.P. Morath, E.A. Garduno, G.D. Jenkins, E. Steenbergen, and V.M. Cowan, "Effects of 63 MeV proton-irradiation on the dark-current in III-V-based, unipolar barrier infrared detectors," *Infrared Physics Techol.*, vol. 97, pp. 448–455, 2019.

[11] G.D. Jenkins, C.P. Morath, and V.M. Cowan, "*In-situ* minority carrier recombination lifetime measurements at radiation sites for rad-hard IR detector materials," *Proc. SPIE*, vol. 9226, no. 92260S, 2014.

[12] ——, "Empirical trends of minority carrier recombination lifetime vs proton radiation for rad-hard IR detector materials," *Proc. SPIE*, vol. 9616, no. 96160G1-9, 2015.

[13] L. Hoglund *et al.*, "Influence of proton radiation on the minority carrier lifetime in midwave InAs/InAsSb superlattices," *Appl. Physics Lett.*, vol. 108, no. 2, p. 263504, 2016.

[14] G.D. Jenkins, C.P. Morath, and V.M. Cowan, "An empirical study of the disparity in rad-tolerance of the minority carrier lifetime between II-VI and III-V space- detector technologies in the MWIR," *J. Electron. Materials*, vol. 46, no. 9, pp. 5405–5410, 2017.

[15] L. Casias, "Transport in MWIR p- and n-type InAsSb and InAs/InAsSb Type II strained layer superlattices for infrared detection," Ph.D. dissertation, Dept. Elect. Eng., UNM, Albuquerque, NM, 2019.

[16] L.K. Casias *et al.*, "Substrate-removed metal-semiconductor-metal device structure to measure vertical carrier transport in strain-balanced InAs/InAsSb Type-II superlattice material," *Appl. Physics Lett.*, 2019, to be published.

[17] P. Martyniuk, M. Kopytko, and A. Rogalski, "Barrier infrared detectors," *Opto-electronics Rev.*, vol. 22, no. 2, pp. 127–146, 2014.

[18] A. Rogalski and P. Martyniuk, "Mid-wavelength infrared nBn for HOT detectors," *J. Electron. Materials*, vol. 43, no. 8, pp. 2963–2969, 2014.

[19] A. White, "Infrared detectors," U.S. Patent 4,679,063, 1983.

[20] D. Rhigher, *private communication*, 2016.

[21] M.D. Peterson, "Numerical simulation of the performance characteristics, instability, and effects of band gap grading in cadmium telluride photovoltaic devices," M.S. thesis, ISU, Ames, IA, 2001.

[22] C. Claeys and E. Simoen, *Radiation Effects in Advanced Semiconductor Materials and Devices*, Springer, 2002.

[23] J.E. Hubbs, G.A. Dole, and M.E. Gramer, *private communication*, 2017.

[24] J.E. Hubbs *et al.*, "Lateral diffusion length changes in HgCdTe detectors in a proton environment," *IEEE Trans. Nucl. Sci.*, vol. 54, no. 6, pp. 2435–2443, 2007.

[25] M.H. Weiler and G.J. Tarnowski, "Characterization of HgCdTe P-on-n heterojunction photodiodes and their defects using variable-area test structures," *J. Electron. Materials*, vol. 26, no. 6, pp. 635–642, 1997.

[26] F.V. de Wiele, "Photodiode quantum efficiency," in *Proc. Nato Advanced Study Inst. on Solid State Imaging*, P.G. Jespers, F. van de Wiele, and M.H. White, Eds., Belgium, 1975, pp. 47–90.

[27] B. Olson *et al.*, "Vertical hole transport and carrier localization in InAs/InAsSb Type-II superlattice heterojunction bipolar transistors," *Physical Rev. Appl.*, vol. 7, p. 024016, 2017.